

Intergrowth Structure of Zeolite Crystals and Pore Orientation of Individual Subunits Revealed by Electron Backscatter Diffraction/Focused Ion Beam Experiments**

Eli Stavitski, Martyn R. Drury,* D. A. Matthijs de Winter, Marianne H. F. Kox, and Bert M. Weckhuysen*

Zeolites are of tremendous scientific and technological importance, since a number of processes in modern chemical industry, such as crude oil refining, rely on their unique combination of catalytic activity and shape selectivity.^[1–3] Consequently, significant efforts have been directed at obtaining in-depth insight into the molecular processes taking place within zeolite pores during catalysis.^[4–6] A popular strategy is to investigate large zeolite crystallites, which are well-defined, ordered, and reproducible and can be used as model systems for diffusion and catalysis studies.^[7–15] However, this task is complicated by the complex structure of zeolite crystals comprising several intergrown building blocks. The interfaces of these subunits may constitute diffusion boundaries due to potential mismatch in the alignment of the microporous network,^[16] and this can render certain regions of the zeolite crystals inaccessible for reactant molecules and consequently affect the catalytic activity of the material.^[8,10,17]

Several methods have been proposed to clarify the intergrowth structure of zeolite crystallites with sizes from micrometers to hundreds of micrometers. These include optical and interference microscopic investigation of the molecular diffusion of guest molecules in the zeolite pores.^[7,8] Recently, we developed an alternative method based on in situ mapping of the template-removal process in individual

zeolite crystals.^[18] The formation of light-absorbing and -emitting species during the calcination process was followed by a combination of optical and confocal fluorescence microscopy. Preferential accumulation of the template decomposition products due to diffusion barriers at the subunits boundaries allowed the architecture of these individual building blocks to be observed. This concept has been successfully applied to four different crystals, namely, CrAPO-5 and SAPO-5 (AFI structure), SAPO-34 (CHA structure), and ZSM-5 (MFI structure). Although this method sheds light onto the organization of the subunits making up a crystal, it does not provide information on pore alignment within the individual subunits. This calls for a characterization method capable of probing local crystal orientation. The electron backscattering diffraction (EBSD)/scanning electron microscopy (SEM) technique is a promising approach that can determine crystal orientation with a spatial resolution of a few tens to hundreds of nanometers.^[19,20] The EBSD patterns are obtained from the surface of small particles or from mechanically polished bulk samples. A recent innovation is the combination of EBSD with focused ion beam (FIB) sectioning in dual-beam microscopes, which allows three-dimensional reconstruction of crystalline microstructures.

Here the first EBSD–FIB study of zeolite crystals, aimed at unraveling the orientation of the complex zeolite channel network, is reported. We illustrate the strength of the approach by attempting to resolve the disagreement over the intergrowth structure of one of the most widely studied micrometer-sized zeolite crystals, namely, coffin-shaped ZSM-5 crystals. ZSM-5 belongs to the MFI structure type and has a two-dimensional channel system with 5.3×5.1 Å straight pores intersected by 5.6×5.3 Å zigzag pores.^[21] Two contradicting models have been proposed for the intergrowth structure of these crystals. The first, coined the two-component model, could be regarded as two interpenetrating crystals rotated by 90° around the common *c* axis. This model consists of two central and four side pyramidal subunits (Figure 1 a). This model was proposed on the basis of an early XRD study^[22] and was further corroborated by optical microscopy results^[7,23] and by experiments in which the crystals were disassembled into single crystalline fragments by ultrasonic treatment.^[24] In the so-called three-component model (Figure 1 b), the crystallographic axes maintain the same orientation across the entire crystal. This model was deduced from the investigation of structural features detected on the crystal surface by atomic force microscopy (AFM).^[25] A small subunit in the middle of the crystals was proposed to

[*] Dr. E. Stavitski, M. H. F. Kox, Prof. Dr. B. M. Weckhuysen
Inorganic Chemistry and Catalysis Group
Department of Chemistry
Utrecht University
Sorbonnelaan 16, 3584 CA Utrecht (The Netherlands)
Fax: (+31) 302–511–027
E-mail: b.m.weckhuysen@uu.nl

Dr. M. R. Drury
Department of Earth Sciences
Utrecht University
P.O. Box 80021, 3508 TA Utrecht (The Netherlands)
Fax: (+31) 302–535–108
E-mail: martynd@geo.uu.nl

D. A. M. de Winter
Cellular Architecture and Dynamics
Faculty of Science
Utrecht University
Padualaan 8, 3584 CH Utrecht (The Netherlands)

[**] We thank the Dutch National Science Foundation (NWO-CW VICI and TOP grants and NWO Large Investment Subsidy for the Dual-Beam Microscope) and the Research School Combination Catalysis (NRSC-C) for financial support.

Supporting information for this article is available on the WWW under <http://dx.doi.org/10.1002/anie.200801433>.

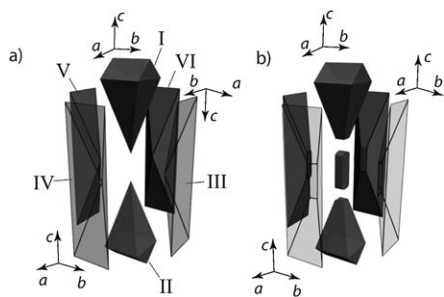


Figure 1. “Exploded” representation of a) two-component and b) three-component models of coffin-shaped ZSM-5 crystals. Orientations of crystal axes in the individual subunits are given. Subunits in the two-component models are denoted I–VI (see text). The straight pores align with the *b* crystal axis, whereas the zigzag pores extend along the *a* crystal axis.

serve as a nucleation seed. As yet there is no clear-cut evidence for either model. The present study aims at resolving this issue.

In the first set of experiments, SEM images of coffin-shaped ZSM-5 crystals with dimensions $100 \times 20 \times 20 \mu\text{m}^3$ were taken, and EBSD patterns were obtained from different spots on the top surface (Figure 2). Since zeolites have low densities ($< 2 \text{ g cm}^{-3}$) and are made of light elements, they are poor electron scatterers, and thus to date only one report on EBSD of zeolites exists, whereby fine mechanical polishing of the polycrystalline zeolite surface was required to obtain diffraction patterns of reasonable quality.^[26] Fortunately, in the present study the very flat growth surfaces of the crystals were suitable for EBSD. Two distinct diffraction patterns were recorded. The first, shown in Figure 2 b, originates from the triangular section at the edge of the crystals, where subunits I or II are exposed (spots A and B), whereas the second diffraction pattern, shown in Figure 2 c, remains unchanged across the crystal body (subunit III, spots C–F) between the terraces visible on the top surface. As mentioned above, zeolites give rather weak diffraction patterns. However, due to the sensitivity of zeolites to the electron beam, enhancing the signal-to-noise ratio by increasing the data-collection time is hardly possible. Therefore, automated recognition of the diffraction bands by the software could not be performed. Nevertheless, after the bands were selected manually, we were able to index the patterns with an orthorhombic structure of ZSM-5,^[27] as shown in Figure 2 d and e. Unambiguous indexing of the patterns is possible if certain diffraction bands, either the {133}-, {804}-, or {151}-type bands, could be recognized. The EBSD patterns could be indexed with the orthorhombic structure both with and without template molecules. The presence or absence of template has a small effect on the relative intensity of the diffraction bands, but does not change their geometry. Crystal orientations obtained from the indexed EBSD patterns indicate that, at the ends of the samples, the crystal axes are rotated by 90° about the common *c* axis (Figure 2 f), consistent with the two-component model (Figure 1 a). This implies that the straight pores are open to the surface of the triangular end of the sample, whereas in the central region of the crystal they run parallel to the top plane of the crystal

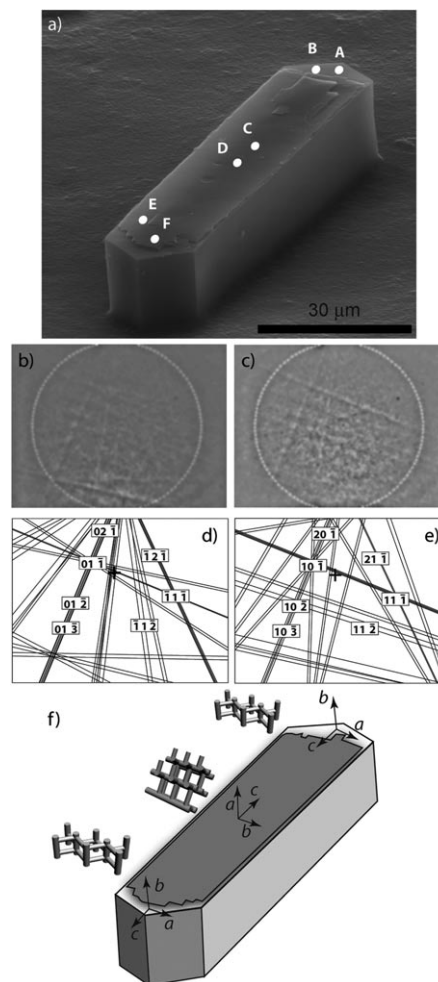


Figure 2. a) SEM image of the coffin-shaped ZSM-5 crystals. Spots where EBSD patterns were taken are marked A–F. b) Diffraction pattern recorded from spot A. c) Diffraction pattern recorded from spot D, which is representative of the body of the crystal (other spots yielded identical patterns). d, e) Indexed patterns from (b) and (c), respectively. f) Crystal orientation at the end and at the main body of the crystal, obtained from indexing. Orientation of the zeolite pores in different regions of the crystals is also shown.

(Figure 2 f). Three crystals were investigated for each orientation shown in Figure 2 a and yielded identical results. In addition, in line with the model, the pore orientation in subunits IV and VI was shown to be identical to that in III and V, as described in the Supporting Information.

Structural information obtained from the surface appears to favor the two-component model; however, further evidence could be obtained if the EBSD technique were extended to the third dimension. To achieve this, the crystal was sectioned by FIB milling. This technique allows material to be removed on the micro- and nanoscale to expose regions of interest which can be subsequently examined by electron microscopy or EBSD. Accelerated ions colliding with the surface cause a collision cascade. The momentum of the primary ion is partially transferred to surface atoms, which are ejected into the vacuum. By varying ion beam parameters that is, the energy, current, and the angle of incidence, as well as

the exposure time, a controlled amount of material can be removed.

Due to the fragility of the porous zeolite structure, conventional top-down milling resulted in complete amorphization of the surface, as no diffraction patterns were discernible after this treatment. Therefore, milling was carried out with the sample rotated so that the ion beam milled parallel to the surface of interest. With this configuration, the crystal was sectioned along its short axis (Figure 3 a,b).

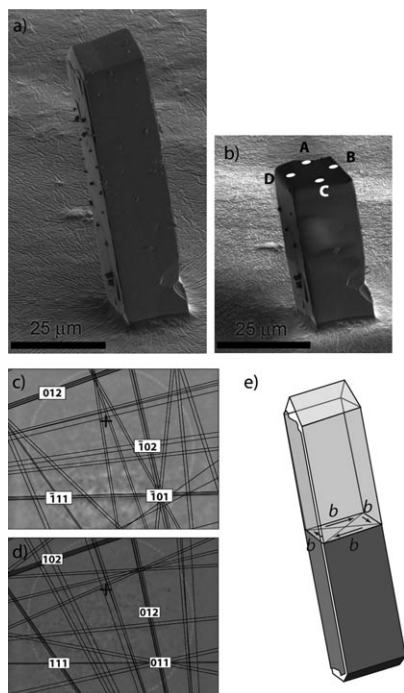


Figure 3. ZSM-5 crystal a) before and b) after ion milling perpendicular to the long crystal axis. c, d) Diffraction patterns obtained from spots A and B, respectively, together with the indexed patterns. e) Crystal orientation in the area exposed after FIB milling. Only the direction of the *b* axis is indicated for clarity.

Milling completely removes subunit I and leaves sections of subunits II–V open to the surface. Indexed diffraction patterns recorded from the surface exposed by milling are shown in Figure 3c. The patterns from the ion-milled surface are weaker than those from the crystal surface, and not all patterns could be unambiguously indexed. Patterns obtained from spots B and D were identical and different to the pattern from point A. Indexing of the patterns revealed that in all three spots the *b* axis is parallel to the crystal side faces, and the *c* axis parallel to the long axis of the crystal (Figure 3e). The latter finding fully supports the two-component model of the ZSM-5 crystal (Figure 1a). In addition, two more FIB sections across the long axis of the crystal in Figure 3a resulted in the same patterns.

Our EBSD–FIB results on crystal orientations combined with confocal fluorescence microscopy observations of the intergrowth boundaries fully confirm the two-component model for the ZSM-5 crystals studied here. The intergrowth structure obtained in the present study is also in full agree-

ment with our recent results on spatially resolved catalytic reactivity in these crystals, as revealed by synchrotron IR and UV/Vis microspectroscopy.^[15,28] More specifically, both techniques were applied to map the formation of the reaction products of acid-catalyzed styrene oligomerization in individual ZSM-5 crystals. We have shown that, when either polarized IR or UV/Vis light was used for absorption measurements, the intensity of the spectral bands due to the carbocationic dimeric and trimeric products was sensitive to the direction of polarization of the light. While the intensity of the absorption bands recorded at the body of the crystal varied drastically on polarization rotation, only slight changes were observed at the edges. Using the two-component model we succeeded in rationalizing the findings by assuming that the elongated styrene dimers and trimers are likely to be aligned within the straight channels. Other evidence in favor of the two-component model is a polarized-light IR study of *p*-xylene adsorbed in MFI crystals.^[29] When the edge areas were probed, the strong IR bands associated with the transition moment along the *z* direction (long axis of *p*-xylene molecule) were found to be inactive, that is, the molecules are aligned collinear with the incident radiation. In the central area, these bands emerged in the spectra, and strong dependence on the polarization of the IR light was observed. Given that *para*-substituted benzenes are preferentially aligned with the straight pores,^[30] these results can be explained by a pore orientation consistent with the two-component model.

In conclusion, we applied the EBSD–FIB method to determine the three-dimensional intergrowth structure and crystal orientation of zeolite crystals, despite their low conductivity and beam sensitivity. The successful demonstration of this approach on large ZSM-5 crystals revealed a two-component intergrowth structure. The EBSD–FIB method may be especially powerful when combined with confocal fluorescence microscopy.^[18] With these two techniques at hand, one can first obtain information on the subunit architecture by fluorescence mapping, mill the crystal by FIB to expose the regions of interest, and finally determine the crystal orientation and pore alignment in the individual building blocks from the EBSD patterns. Beyond structure determination of zeolite crystals, the technique can be applied, for example, to zeolite membranes in order to visualize their microtexture and to predict their performance. The EBSD–FIB technique provides new opportunities in studying zeolite crystals in particular and crystalline catalyst materials in general.

Received: March 26, 2008

Published online: June 20, 2008

Keywords: crystal intergrowth · electron diffraction · heterogeneous catalysis · ion beam milling · zeolites

[1] H. F. Rase, *Handbook of Commercial Catalysts: Heterogeneous Catalysts*, CRC, Boca Raton, 2000.

[2] J. Hagen, *Industrial Catalysis: A Practical Approach*, Wiley-VCH, Weinheim, 2006.

- [3] U. Dingerdissen, A. Martin, D. Herein, H. J. Wernicke in *Handbook of Heterogeneous Catalysis, Vol. 1* (Eds.: G. Ertl, H. Knözinger, F. Schüth, J. Weitkamp), Wiley-VCH, Weinheim, **2008**, p. 37.
- [4] A. Corma, *Chem. Rev.* **1995**, *95*, 559; A. Corma, M. Diaz-Cbanas, J. Martinez-Triguero, F. Rey, J. Rius, *Nature* **2002**, *418*, 6897.
- [5] *Catalysis and Zeolites: Fundamentals and Applications* (Eds.: J. Weitkamp, L. Puppe), Springer, Heidelberg, **1999**.
- [6] *Introduction to Zeolite Science and Practice* (Eds.: H. van Bekkum, P. A. Jacobs, E. M. Flanigen, J. C. Jansen), Elsevier, Amsterdam, **2001**.
- [7] M. Kocirik, J. Kornatowski, V. Masarik, P. Novak, A. Zikanova, J. Maixner, *Microporous Mesoporous Mater.* **1998**, *23*, 295.
- [8] E. Lehmann, C. Chmelik, H. Scheidt, S. Vasenkov, B. Staudte, J. Karger, F. Kremer, G. Zadrozna, J. Kornatowski, *J. Am. Chem. Soc.* **2002**, *124*, 8690.
- [9] Y. S. Lin, N. Yamamoto, Y. Choi, T. Yamaguchi, T. Okubo, S. I. Nakao, *Microporous Mesoporous Mater.* **2000**, *38*, 207.
- [10] O. Geier, S. Vasenkov, E. Lehmann, J. Karger, U. Schemmert, R. A. Rakoczy, J. Weitkamp, *J. Phys. Chem. B* **2001**, *105*, 10217.
- [11] G. Müller, J. Bodis, J. Kornatowski, *Microporous Mesoporous Mater.* **2004**, *69*, 1.
- [12] M. H. F. Kox, E. Stavitski, J. C. Groen, J. Pérez-Ramírez, F. Kapteijn, B. M. Weckhuysen, *Chem. Eur. J.* **2008**, *14*, 1718.
- [13] M. B. J. Roeffaers, B. F. Sels, H. Uji-i, B. Blanpain, P. L'hoëst, P. A. Jacobs, F. C. De Schryver, J. Hofkens, D. E. De Vos, *Angew. Chem.* **2007**, *119*, 1736; *Angew. Chem. Int. Ed.* **2007**, *46*, 1706.
- [14] J. Kärger, P. Kortunov, S. Vasenkov, L. Heinke, D. R. Shah, R. A. Rakoczy, A. Traa, J. Weitkamp, *Angew. Chem.* **2006**, *118*, 8010; *Angew. Chem. Int. Ed.* **2006**, *45*, 7846.
- [15] E. Stavitski, M. H. F. Kox, I. Swart, F. M. F. de Groot, B. M. Weckhuysen, *Angew. Chem.* **2008**, *120*, 3599; *Angew. Chem. Int. Ed.* **2008**, *47*, 3543.
- [16] D. G. Hay, H. Jaeger, K. G. Wilshier, *Zeolites* **1990**, *10*, 571.
- [17] G. Müller, T. Narbeshuber, G. Mirth, J. A. Lercher, *J. Phys. Chem.* **1994**, *98*, 7436.
- [18] L. Karwacki, E. Stavitski, M. H. F. Kox, J. Kornatowski, B. M. Weckhuysen, *Angew. Chem.* **2007**, *119*, 7366; *Angew. Chem. Int. Ed.* **2007**, *46*, 7228.
- [19] D. J. Dingley, V. Randle, *J. Mater. Sci.* **1992**, *27*, 4545.
- [20] F. J. Humphreys, *J. Mater. Sci.* **2001**, *36*, 3833.
- [21] G. T. Kokotailo, S. L. Lawton, D. H. Olson, W. M. Meier, *Nature* **1978**, *272*, 437.
- [22] G. D. Price, J. J. Pluth, J. V. Smith, J. M. Bennett, R. L. Patton, *J. Am. Chem. Soc.* **1982**, *104*, 5971.
- [23] C. Weidenthaler, R. X. Fischer, R. D. Shannon, O. Medenbach, *J. Phys. Chem.* **1994**, *98*, 12687.
- [24] W. Schmidt, U. Wilczok, C. Weidenthaler, O. Medenbach, R. Goddard, G. Buth, A. Cepak, *J. Phys. Chem. B* **2007**, *111*, 13538.
- [25] J. R. Agger, N. Hanif, C. S. Cundy, A. P. Wade, S. Dennison, P. A. Rawlinson, M. W. Anderson, *J. Am. Chem. Soc.* **2003**, *125*, 830.
- [26] G. M. Pennock, A. Barnhoorn, A. J. Bons, M. R. Drury, *J. Mater. Sci. Lett.* **2001**, *20*, 1099.
- [27] H. van Koningsveld, J. C. Jansen, H. van Bekkum, *Zeolites* **1990**, *10*, 235.
- [28] M. H. F. Kox, E. Stavitski, B. M. Weckhuysen, *Angew. Chem.* **2007**, *119*, 3726; *Angew. Chem. Int. Ed.* **2007**, *46*, 3652; E. Stavitski, M. H. F. Kox, B. M. Weckhuysen, *Chem. Eur. J.* **2007**, *13*, 7057.
- [29] F. Schüth, *J. Phys. Chem.* **1992**, *96*, 7493.
- [30] H. Gies, B. Marler, C. Fyfe, G. Kokotailo, Y. Feng, D. E. Cox, *J. Phys. Chem. Solids* **1991**, *52*, 1235.